PHYSICAL REVIEW D **86,** 116013 (2012)

Phase diagram of Nambu–Jona-Lasinio model with dimensional regularization

T. Inagaki
Information Media Center, Hiroshima University, Higashi-Hiroshima, Hiroshima 739-8521, Japan

D. Kimura
Faculty of Education, Hiroshima University, Higashi-Hiroshima, Hiroshima 739-8524, Japan

H. Kohyama
Department of Physics, Chung-Yuan Christian University, Chung-Li 32023, Taiwan

A. Kvinikhidze
A. Razmadze Mathematical Institute of Georgian Academy of Sciences, M. Alexidze Street 1, 380093 Tbilisi, Georgia
(Received 24 April 2012; revised manuscript received 18 November 2012; published 28 December 2012)

Regularization dependence of the Nambu–Jona-Lasinio model leaves room for improvement. To help in choosing a suitable regularization scheme, we investigate the phase diagram on the temperature-chemical potential plane in the Nambu–Jona-Lasinio model with the dimensional regularization. While the structure of the resulting diagram shows resemblance to the one in the frequently used cutoff regularization, some results of our study indicate a striking difference between these regularizations. Diagrams in the dimensional regularization always indicate the first-order phase transition at high chemical potential, while the first-order transition does not occur in the cutoff method for some parameter sets.

DOI: 10.1103/PhysRevD.86.116013 PACS numbers: 11.10.Wx, 11.30.Qc, 12.39.−x

I. INTRODUCTION

The phase diagram of the quark matter has been actively investigated for decades [1]. Quarks are confined inside hadrons and cannot be observed as free particles at low energy. On the other hand, at high energy, quarks become free particles due to the asymptotic freedom of the strong interaction. Therefore, it is expected that quarks undergo the phase transition between confined and deconfined states which is one of the most important issues in theoretical and experimental particle physics.

The fundamental theory to describe quark matter is quantum chromodynamics (QCD), the theory of strong interaction. It is, however, not practical to extract reliable predictions at low energy due to the necessity of complicated nonperturbative calculations in this area. For this reason some effective approaches are used such as the Nambu–Jona-Lasinio (NJL) model [2] and its Polyakov-loop incorporated version, the PNJL model [3], the linear sigma model [4], the chiral perturbation theory [5], and the lattice QCD simulations [6].

In this paper, we will consider the NJL model known as a low-energy effective theory of QCD (for reviews, see, Refs. [7–10]). At low temperature, T, and chemical potential, μ, constituent quarks are heavy due to the chiral symmetry spontaneous breaking, while they are expected to be light at high T and/or μ where the chiral symmetry is getting restored. Thus the quark system is closely related to the phenomenon of the chiral phase transition. The NJL model actually predicts the chiral symmetry breaking at low energy and its restoration at high energy. Many investigations of the phase diagram are based on the NJL and PNJL models (see, e.g., Refs. [11–25]).

Since the NJL model is not renormalizable, the model predictions inevitably depend on a regularization procedure applied. The most frequently used method is probably the three-momentum cutoff regularization which introduces the cutoff scale Λ. The model in the cutoff scheme may miss an important contribution when the quark density becomes comparable to the cutoff scale. There is an alternative method, the dimensional regularization (DR) [19,26–28], to avoid the issue [29]. In the DR, divergences coming from fermion loop integrals are regularized by lowering the dimension of the integration through an analytic continuation in the dimension variable. The DR preserves gauge symmetry and chiral symmetry, as well as Lorentz invariance. Thus the DR method respects more symmetries than the cutoff method.

Using various regularization ways is interesting, because we believe that the regularization scheme is a dynamical part of the NJL model, related to the effective size and shape of the quark interaction as discussed in Ref. [30]. Thus the choice of regularization has direct effect on the reliability of the NJL model. It was found that the model with the DR nicely describes quark systems at low energy, specifically such characteristics as the phase structure and meson properties [29–32]. Note that if we make some assumptions, the Schwinger-Dyson equation coincides with the gap equation in the two-dimensional NJL model at the leading order of $1/N_c$ expansion [33].

We shall study in this paper the phase diagram in the three-flavor NJL model with the DR. It is interesting because the recent work by the present authors [30] indicates that the phase structure, especially the order of the

transition, may differ drastically from the one in the cutoff regularization.

The structure of this paper is as follows: In Sec. II, the three-flavor NJL model and its parameters are presented. Section III is devoted to the explanation on the procedure of drawing the phase diagram. We then display the resulting phase diagram of the model in Sec. IV. We also evaluate the Columbia plot for two regularization methods in Sec. V. The concluding remarks are given in Sec. VI.

II. THREE-FLAVOR NJL MODEL

A. The model

The Lagrangian of the three-flavor model is

$$\mathcal{L}_{\mathrm{NJL}} = \sum_{i,j} \bar{q}_i (i\not{\partial} - \hat{m})_{ij} q_j + \mathcal{L}_4 + \mathcal{L}_6, \tag{1}$$

$$\mathcal{L}_4 = G \sum_{a=0}^{8} \left[\left(\sum_{i,j} \bar{q}_i \lambda_a q_j \right)^2 + \left(\sum_{i,j} \bar{q}_i i\gamma_5 \lambda_a q_j \right)^2 \right], \tag{2}$$

$$\mathcal{L}_6 = -K[\det \bar{q}_i (1-\gamma_5) q_j + \mathrm{H.c.}], \tag{3}$$

where $\hat{m}_{ij}$ represents the diagonal mass matrix $\mathrm{diag}(m_u, m_d, m_s)$ with flavor indices i, j. G and K are the four- and six-fermion couplings, λ_a are the Gell-Mann matrices in flavor space with $\lambda_0 = \sqrt{2/3} \cdot \mathbf{1}$. The determinant in $\mathcal{L}_6$ runs over flavor space, so this leads to the six-point interaction known as the Kobayashi-Maskawa-'t Hooft term [34,35].

The vacuum of the model is determined by the minimum of the thermodynamic potential $\Omega = -\ln Z/(\beta V)$ with the partition function Z, the inverse temperature $\beta = 1/T$, and the volume of the system V. Applying the mean-field approximation, we can calculate the potential Ω in the imaginary time formalism,

$$\Omega = \Omega_v + \Omega_0 + \Omega_T, \tag{4}$$

$$\Omega_v = 2G(\phi_u^2 + \phi_d^2 + \phi_s^2) - 4K\phi_u\phi_d\phi_s, \tag{5}$$

$$\Omega_0 = -\frac{2^{D/2} N_c}{2} \int \frac{d^{D-1}p}{(2\pi)^{D-1}} [E_u + E_d + E_s], \tag{6}$$

$$\Omega_T = -\frac{2^{D/2} N_c}{2} T \int \frac{d^{D-1}p}{(2\pi)^{D-1}} \sum_{i,\pm} \ln[1 + e^{-\beta E_i^{\pm}}]. \tag{7}$$

Here Ω_v corresponds to the vacuum contribution by the chiral condensates, Ω_0 and Ω_T denote the temperature-independent and -dependent contributions, $\phi_i (\equiv \langle \bar{i}i \rangle)$ is the chiral condensate for each quark which is the order parameter of the model, and $N_c (= 3)$ is the number of colors. D denotes dimensions in the fermion loop integral, $E_i = (p^2 + m_i^{*2})^{1/2}$ is the energy of the quasiparticle with the constituent quark mass m_i^*, $E_i^{\pm} = E_i \pm \mu$ with a quark chemical potential $\mu (= \mu_u = \mu_d = \mu_s)$.

The fermion loop integral in Eq. (6) diverges, therefore we will perform the analytic continuation in D to regularize it by decreasing the dimension D as discussed in Refs. [30,31]. In the cutoff scheme, the divergent contribution is dropped by introducing the momentum cutoff Λ. To be more precise, the regularization in the DR and cutoff schemes is performed by the following replacements

$$\int \frac{d^{D-1}p}{(2\pi)^{D-1}} \to \frac{2(4\pi)^{-(D-1)/2}}{\Gamma[(D-1)/2]} M_0^{4-D} \int_0^{\infty} dp p^{D-2}, \tag{8}$$

$$\int \frac{d^{D-1}p}{(2\pi)^{D-1}} \to \frac{1}{2\pi^2} \int_0^{\Lambda} dp p^2, \tag{9}$$

where M_0 is the renormalization scale that is needed to render physical quantities in correct mass dimensions.

As mentioned in the Introduction, the constituent quark mass

$$m_i^* = m_i - 4G\phi_i + 2K\phi_j\phi_k, \qquad (i \neq j \neq k \neq i) \tag{10}$$

is closely related to the chiral symmetry breaking, namely to the value of ϕ_i. The self-consistent gap equations (10) are obtained as the condition for the thermodynamic potential to be at the extremum, $\partial\Omega/\partial\phi_i = 0$. Equations (10) explicitly show that the difference between constituent and current quark masses is due to the underlying chiral symmetry breaking.

It is worth mentioning that the anomalous $\mathrm{U_A}(1)$ transformation can be used to ensure that all quark masses are positive. However, the $\mathrm{U_A}(1)$ transformation leads the positive chiral condensates which are not consistent with the study of QCD sum rules [36]. The sign of the mass should be studied when considering CP-violating gauge couplings [37]. The detailed arguments on the $\mathrm{U_A}(1)$ transformation and the CP problem are discussed in the Appendix. The sign of the constituent quark masses does not change the phase diagram of the chiral transition in the NJL model.

Note that the constituent quark masses can be positive if one performs the renormalization by introducing counterterms which are necessary to eliminate the divergences coming form loop integrals [38]. However, the renormalized models in DR generate results similar to those in the cutoff method, which is not of interest in this paper.

B. Model parameters

The NJL model with the DR has seven free parameters: current quark mass m_u, m_d, m_s, the four- and six-point couplings G, K, the dimension D, and the renormalization scale M_0.

We consider, for simplicity, the isospin symmetric case, $m_d = m_u$, and set several values for $m_u (= 3, 4, 5, 5.5, 6$ MeV). We then fix the remaining parameters by

TABLE I. Case m_η^{LD}.

m_u	m_s	G	K	M_0	D
3.0	84.9	-0.0195	9.02×10^{-7}	118	2.29

TABLE II. Case m_η.

m_u	m_s	G	K	M_0	D
3.0	79.0	-0.0130	2.29×10^{-7}	107	2.37
4.0	106	-0.00748	8.26×10^{-8}	92.0	2.52
5.0	134	-0.00357	1.99×10^{-8}	73.2	2.69
5.5	147	-0.00231	8.40×10^{-9}	62.4	2.77
6.0	162	-0.00142	3.23×10^{-9}	50.9	2.87

TABLE III. Case χ.

m_u	m_s	G	K	M_0	D
3.0	77.1	-0.0168	2.23×10^{-7}	120	2.28
4.0	106	-0.0143	2.11×10^{-7}	116	2.36
5.0	134	-0.0119	1.80×10^{-7}	112	2.43
5.5	150	-0.0109	1.62×10^{-7}	110	2.47
6.0	166	-0.00992	1.48×10^{-7}	109	2.50

choosing five physical quantities from among those listed below:

$$\begin{aligned} m_\pi &= 138\ \mathrm{MeV}, \qquad f_\pi = 92\ \mathrm{MeV}, \\ m_{\mathrm{K}} &= 495\ \mathrm{MeV}, \qquad m_{\eta'} = 958\ \mathrm{MeV}, \\ m_\eta &= 548\ \mathrm{MeV}, \qquad \chi^{1/4} = 170\ \mathrm{MeV}. \end{aligned} \tag{11}$$

Following Ref. [30], we name the parameter sets as case χ and m_η depending on which quantities are selected. Case χ (m_η) is fitted by $\{m_\pi, f_\pi, m_{\mathrm{K}}, m_{\eta'}, \chi(m_\eta)\}$. The parameter setting was performed in Ref. [31], and we shall employ three parameter sets, Case m_η^{LD}, m_η and χ, which are shown in Tables I, II, and III. Note that case m_η has two parameter sets for $m_u = 3$ MeV; to distinguish between them, we use the superscript LD (lower dimension).

For the sake of comparison we also align the parameters of the cutoff case in Table IV. In the cutoff case, we fix four parameters, m_s, G, K and Λ with $\{m_\pi, f_\pi, m_{\mathrm{K}}, m_{\eta'}\}$. Unfortunately, there is no solution to simultaneously reproduce the above listed quantities for $m_u \gtrsim 5.87$ MeV.

III. CRITICAL BEHAVIOR

In this section we explain how to draw the phase diagram of the model through the analysis of the thermodynamical potential and the gap equations.

A critical temperature T_c or chemical potential μ_c are given by the maxima of

$$\frac{\partial \phi_u}{\partial t}, \qquad (t = T \quad \text{or} \quad \mu). \tag{12}$$

To be precise, in the case of $t = T$, the critical temperature, T_c, is given by a value of T at which the two-variable function, $\partial\phi_u(\mu, T)/\partial T$, reaches the maximum. Thus the critical temperature, $T_c = T_c(\mu)$, is a function of μ. The critical chemical potential, $\mu_c(T)$, is defined analogously.

We apply $t = T(\mu)$ for low μ (T) in the crossover region. The above quantity, $\partial\phi_u/\partial T$, becomes infinite at $T_c(\mu_c)$ when the transition is of the first order. In this case we determine the transition boundary by the point where the discontinuous change of the chiral condensate ϕ_u occurs by directly searching the minimum of the thermodynamic potential. It is obvious that this procedure is consistent with the criterion of Eq. (12), because a divergent point coincides with the maximum point.

A. Thermodynamic potential

To see the tendency of the phase transition, we show the behavior of $\Omega(= \Omega(\phi_u, \phi_s) - \Omega(0, 0))$ for the cases m_η and cutoff, with $m_u = 4$ MeV near the transition boundary in Fig. 1. The curves are plotted along the line $\phi_s = 0.36\phi_u + 0.83\phi_u^0$ for $T = 10$, 75 and 85 MeV with $\mu = 480$ MeV in the upper panel, and along the line

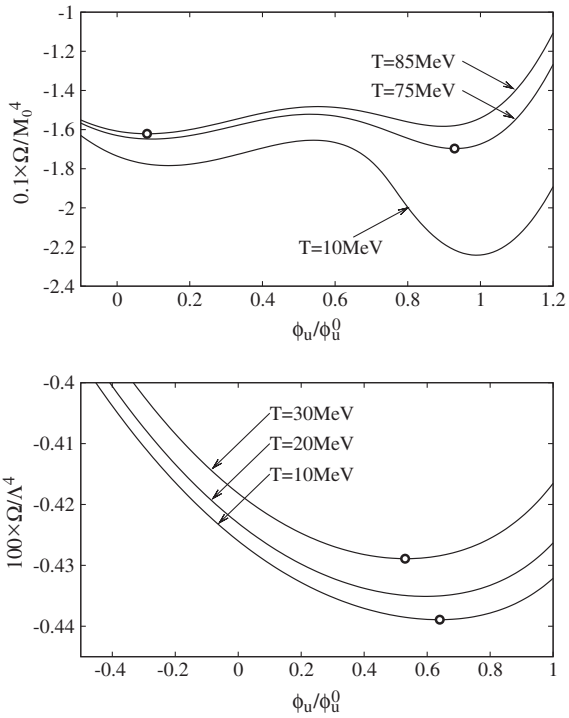

FIG. 1. Upper panel: $0.1 \cdot \Omega/M_0^4$ along the line $\phi_s = 0.36\phi_u + 0.83\phi_u^0$ in case m_η with $m_u = 4$ MeV for $T = 10$, 75, 85 MeV and $\mu = 480$ MeV. Lower panel: $100 \cdot \Omega/\Lambda^4$ along the line $\phi_s = 0.103\phi_u + 1.43\phi_u^0$ in the case Cutoff with $m_u = 4$ MeV for $T = 10$, 20, 30 MeV and $\mu = 290$ MeV. Here $\Omega = \Omega(\phi_u, \phi_s) - \Omega(0, 0)$ and ϕ_u^0 denotes the chiral condensate at T, $\mu = 0$ for each case. The circles indicate the global minima.

TABLE IV. Case Cutoff.

m_u	m_s	$G\Lambda^2$	$K\Lambda^5$	Λ
3.0	89.5	1.55	8.34	960
4.0	110	1.60	8.38	797
5.0	128	1.71	8.77	682
5.5	136	1.81	9.17	630
5.87	139	2.09	10.1	580

$\phi_s = 0.103\phi_u + 1.43\phi_u^0$ for $T = 10$, 20, 30 MeV with $\mu = 290$ MeV in the lower panel. These lines are chosen so as to show the global minima for lower $T = 75(10)$ MeV and higher $T = 85(30)$ MeV, which are indicated by the circles, near the transition temperature $T_c \simeq 80(20)$ MeV. ϕ_u^0 denotes the chiral condensate ϕ_u at T, $\mu = 0$ for each case.

There exists a bump between two stable minima in the DR case, which means that the transition is of the first order between $T = 75$ and 85 MeV for $m_u = 4$ MeV in the Case m_η. The shape of the potential with a bump does not change drastically if one chooses different parameter sets. On the other hand, the cutoff case (lower panel) produces rather monotonous curves with no bump when we choose the parameter sets with a small value of m_u, which leads to a smooth crossover. This different tendency may stem from the fact that the ratio of the thermal contribution (μ dependence) $\Omega_T/(\Omega_v + \Omega_0)$ in the DR case is larger than that in the cutoff case at low T.

B. $\partial\phi_u/\partial T$

In the crossover region, it is technically easier to analyze Eq. (12) through solving the gap equations because ϕ_u changes continuously with respect to $T(\mu)$. We show the numerical results in Fig. 2. One sees that the maximum point moves toward lower T with increasing μ, and the peak becomes large at high μ. The peak actually diverges when T and μ coincide with the critical point (T_{CP}, μ_{CP}). Below T_{CP}, the transition becomes first order, and the analysis by Eq. (12) is no longer practically useful for the determination of the transition boundary as mentioned above.

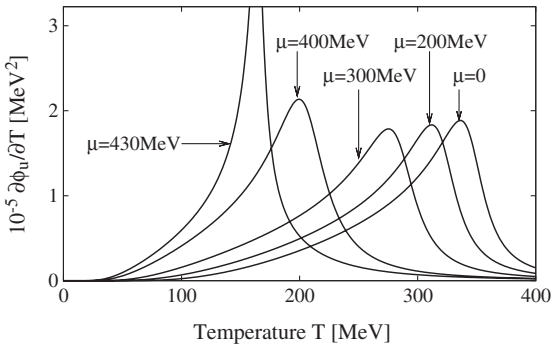

FIG. 2. $\partial\phi_u/\partial T$ in the case m_η with $m_u = 4$ MeV.

IV. PHASE DIAGRAM

We are now ready to discuss the phase structure of the NJL model with the DR.

A. Transition on ϕ_u

Figure 3 displays the typical structure of the phase diagram in the model with the DR in the Case $m_\eta^{\rm LD}$. This is a reasonable picture of a system in the chiral symmetry broken phase at low T and μ, and in the chiral symmetry restored phase at high T and/or μ. The solid (dashed) line represents the first-order (crossover) transition, and the circle indicates the critical point. Note that the transition temperature, $T_c = 184$ MeV for $\mu = 0$, is comparable with the lattice QCD prediction, 150–200 MeV. The critical point is located at $(T_{CP}, \mu_{CP}) = (99\ \text{MeV}, 239\ \text{MeV})$, and it is interesting to see that T_{CP} is close to one obtained in the PNJL model with the cutoff regularization, $T_{CP} = 102$ MeV, for the frequently used parameter set of [9], whereas $T_{CP} = 48$ MeV in the NJL model [24]. Note that the obtained critical point is close to one obtained in a NJL-type model with the smooth form factor [20], $(T_{CP}, \mu_{CP}) = (101\ \text{MeV}, 211\ \text{MeV})$ and in the linear sigma model [39], $(T_{CP}, \mu_{CP}) = (99\ \text{MeV}, 207\ \text{MeV})$. Below we make a more detailed comparison between the DR and the cutoff schemes.

Figure 4 shows the phase diagrams in the cases m_η and χ for various m_u. We note that in the case m_η, the region of the chiral symmetry broken phase becomes smaller with choosing the smaller value of m_u. On the other hand, the case χ produces similar curves for different m_u. The different behavior can be explained by the fact that the constituent quark mass m_u^* gets smaller with decreasing m_u in the case m_η, while it almost does not change in the case χ as discussed in Ref. [31]. In the cutoff case (Fig. 5) the region of the chiral symmetry broken state shrinks when m_u is lowered as observed in case m_η. It is very interesting to

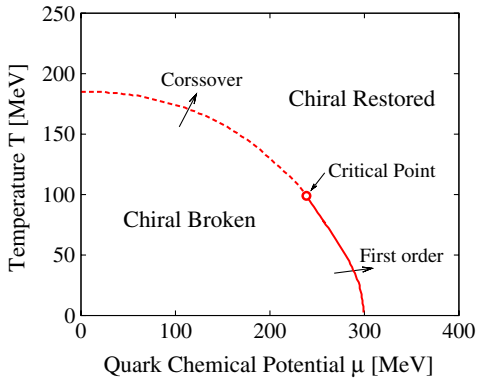

FIG. 3 (color online). Phase diagram in the case $m_\eta^{\rm LD}$ with $m_u = 3$ MeV. The solid (dashed) line represents the first-order (crossover) transition. The circle indicates the critical point.

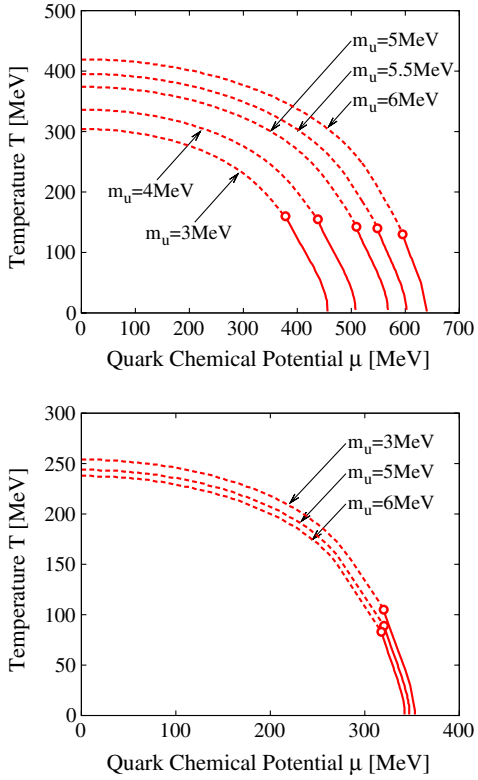

FIG. 4 (color online). Phase diagrams in the cases m_η and χ are shown in the upper and lower panels. The solid (dashed) lines represent the first-order (crossover) transition. The circles indicate the critical points.

note that the critical point disappears below $m_u = 5$ MeV, where the transition is crossover for all T and μ.

A striking difference between the two regularizations is that the critical point moves towards higher temperature with decreasing m_u in the DR, while it moves to the opposite direction in the cutoff case. The difference may be understood by observing the value of the six-point coupling K, which becomes larger (smaller) with decreasing m_u in the DR (cutoff) procedure, since the Kobayashi-Maskawa-'t Hooft term shown in Eq. (3) tends to drive the first-order phase transition [24].

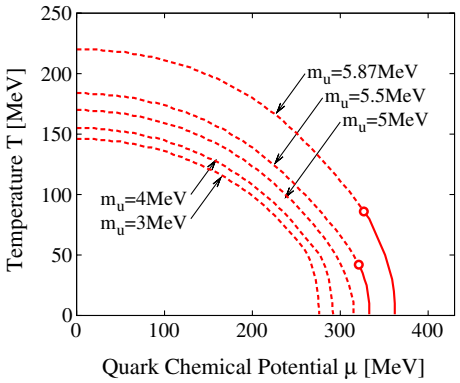

FIG. 5 (color online). Corresponding diagrams in the case Cutoff.

B. Partial transition on ϕ_s

As discussed in Ref. [30], chiral condensates undergo two discontinuous changes at low T in the DR scheme. Figure 6 displays the typical behavior of ϕ_u and ϕ_s as functions of μ at low $T(= 10$ MeV), plotted in the case m_η^{LD} with $m_u = 3$ MeV. One clearly observes two gaps: one is located around $\mu_c^{(u)} \simeq 300$ MeV and the other is around $\mu_c^{(s)} \simeq 365$ MeV. Here we call these discontinuities as first and second gaps for lower and higher chemical potential, respectively. The first gap comes from the effect of the approximate $\mathrm{SU_L}(2) \otimes \mathrm{SU_R}(2)$ restoration and the second one comes from that of the partial $\mathrm{SU_L}(3) \otimes \mathrm{SU_R}(3)$ restoration. Two gaps are also observed in the NJL model with the cutoff regularization under the charge neutrality condition [40]. Thus it may be interesting to study the phase structure concerning the second transition as well.

To draw the phase diagram on the second transition, we set the criterion of the transition by using the following quantity

$$\frac{\partial \phi_s}{\partial t}, \qquad (t = T \quad \text{or} \quad \mu). \tag{13}$$

Then below μ_{CP}, namely in the crossover region, the above quantity has only one maximum, which determines the crossover transition on ϕ_s. While above μ_{CP}, the quantity $\partial\phi_s/\partial\mu$ shows nontrivial behavior; it becomes infinite at $\mu_c^{(u)}$ and has second maximum at $\mu_c^{(s)}$. So $\partial\phi_s/\partial\mu$ has typical two maxima at $\mu_c^{(u)}$ and $\mu_c^{(s)}$ below T_{CP}, as seen in Fig. 6. Here we call the transition point corresponding to the second maximum $\mu_c^{(s)}$, "the second phase boundary." To distinguish between the two phase transitions, we call the transition line on ϕ_u, discussed in the previous subsection, "the first phase boundary."

In the phase diagram on the first and second phase boundaries (Fig. 7), the dashed and dotted lines represent the crossover transition on ϕ_u and ϕ_s, respectively.

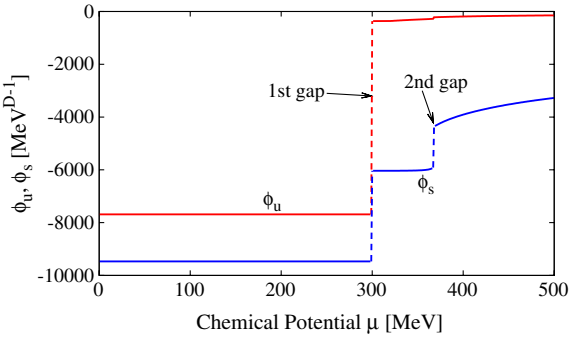

FIG. 6 (color online). Chiral condensates ϕ_u and ϕ_s for $T = 10$ MeV in the case m_η^{LD} with $m_u = 3$ MeV.

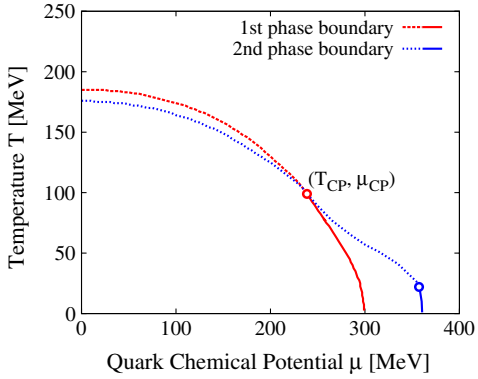

FIG. 7 (color online). The first and second phase boundaries in the case m_η^{LD} with $m_u = 3$ MeV. The dashed and dotted lines represent the crossover transition on ϕ_u and ϕ_s. The solid lines indicate the transition on the first and second gap, respectively. The circles exhibit the critical points.

The solid line for lower (higher) chemical potential indicates the discontinuous change on the first (second) gap. We see that the crossover line on ϕ_s is observed at a bit lower temperature than that on ϕ_u for $\mu < \mu_{CP}$. It should be noticed that the critical curves on ϕ_u and ϕ_s intersect at the critical end point (T_{CP}, μ_{CP}) on ϕ_u. Because the value of ϕ_s is affected by ϕ_u, as is clearly seen from Fig. 6, ϕ_s shows discontinuous change at the point where ϕ_u has a gap. Then $\partial\phi_s/\partial t$ blows up and approaches infinity near the critical point where $\partial\phi_u/\partial t$ is divergent. Below T_{CP}, $\partial\phi_s/\partial\mu$ has two maxima appearing at the first gap and higher chemical potential. The first maximum coincides with the red solid line and the second one is plotted by the blue line in Fig. 7. The transition on the second boundary also has the critical point whose location is exhibited by the blue circle at higher chemical potential.

We also studied the other cases, m_η and χ, with various m_u, and found that the qualitative behavior does not show remarkable difference; the critical point on ϕ_s moves toward higher temperature with decreasing m_u as seen in the ϕ_u case. Therefore, we only displayed the case m_η^{LD} here.

V. CRITICAL BOUNDARY

Having obtained the phase diagram for the NJL model in the DR scheme, it may be interesting to discuss the chiral critical boundary, so called Columbia plot [41]. The critical boundary is drawn by searching the order of the phase transition for various m_u and m_s while the remaining parameters discussed in Sec. II B are fixed. Thus the current quark masses, m_u and m_s, are treated as free parameters when one studies the critical boundary.

Figure 8 displays the critical boundary for the cases m_η (upper panel) and cutoff (lower panel) for various m_u. We first note that the values of the critical mass in the DR are considerably smaller than in the cutoff case with $m_u = 5.0$

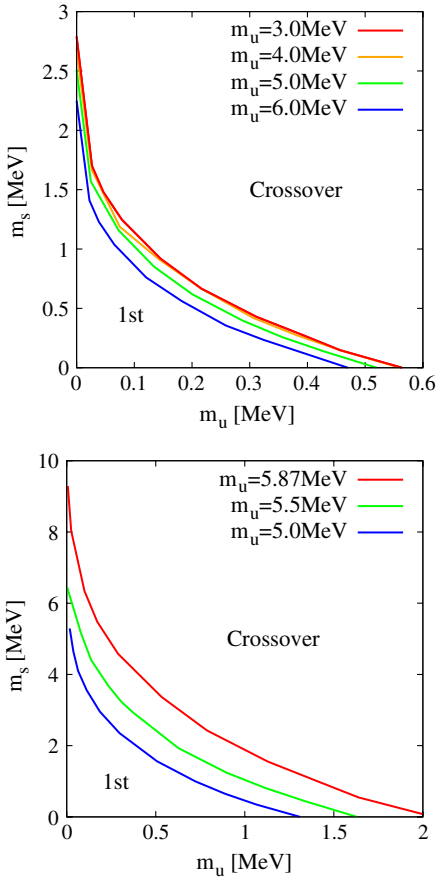

FIG. 8 (color online). The critical boundary for the cases m_η and Cutoff.

and 5.5 MeV. We also note that the region of the first-order phase transition in the case m_η does not depend drastically on the choice of the parameter sets. However, the first-order phase transition region shrinks with decreasing m_u and disappears at $m_u = 4$ MeV in the case Cutoff. This is a sharp contrast seen between the cases with DR and Cutoff regularization.

We have also evaluated the critical boundary for the cases m_η^{LD} and χ and found that the obtained curves indicate similar pictures to those in case m_η. Here we have only shown the results for case m_η.

VI. CONCLUDING REMARKS

We studied the phase diagram of the NJL model with the DR and cutoff regularization. We found that the phase diagram on the T-μ plane in the model with the DR for various parameter sets shows qualitatively similar pictures. The typical transition temperatures are around 170, 350, 250 and 170 MeV in the cases m_η^{LD}, m_η, χ and Cutoff, respectively. The critical points are located around $T_{CP} =$ 100–150 MeV in the DR, and $T_{CP} =$ 50–100 MeV in the cutoff method. Interestingly enough, the temperature of the critical point T_{CP} increases with decreasing m_u in the

DR case, while it rapidly becomes small in the cutoff case as confirmed in Fig. 5. This is a sharp qualitative difference between the two cases.

In Sec. V we drew the Columbia plot for the case of DR and cutoff regularization to study the order of phase transition in more detail. We saw that in the Columbia plot ($\mu = 0$), the cutoff way leads to a larger region of the first-order phase transition than that of the DR. However, the first-order transition region disappears when one chooses the parameter sets with smaller m_u in the cutoff case. On the other hand, the first-order transition region remains in the DR, which is again the distinguishing difference between the two regularizations.

We have also studied the phase structure on the change of ϕ_s in Sec. IV B, where we found that the approximate $\mathrm{SU_L}(2) \otimes \mathrm{SU_R}(2)$ symmetry and the partial $\mathrm{SU_L}(3) \otimes \mathrm{SU_R}(3)$ symmetry restore at a similar temperature for low chemical potential, $\mu < \mu_{CP}$. It may be difficult to distinguish between the two lines experimentally, because the transitions are smooth crossovers at low chemical potential.

From the obtained phase diagrams and the Columbia plot, we conclude that the first-order phase transition persists for low m_u in the model with the DR method. The finding is consistent with the current symmetry analysis–based consensus [42], stating that the chiral phase transition is of the first order in the chiral limit, $m_{u,d,s} \to 0$. This tendency may be understood by the following reasoning. The loop contribution from the lower integration momenta is enhanced by lowering dimension. It introduces nonlocality in the model with the DR. The infrared behavior of the loop integral is important for thermal corrections. It can raise the critical end-point temperature, T_{CP}.

Finally, because the parameter difference crucially affects the location of the critical point as confirmed in this paper, we think it is interesting to study the related issues, such as the case with the chiral limit and the analysis in the next-to-leading order approximation of the $1/N_c$ expansion.

ACKNOWLEDGMENTS

H. K. is supported by Grant No. NSC-99-2811-M-033-017 from the National Science Council (NSC) of Taiwan. A. K. was supported by the Georgian Shota Rustaveli National Science Foundation (Grant No. 11/31).

APPENDIX: $\mathrm{U_A}(1)$ AND STRONG *CP* VIOLATION

We start from a primordial θ term,

$$\mathcal{L}_\theta = \frac{g_s^2}{16\pi^2}\theta\epsilon^{\mu\nu\rho\sigma}F^a_{\mu\nu}F^a_{\rho\sigma}, \tag{A1}$$

where $F^a_{\mu\nu}$ is the field strength for gluons, and g_s is the strong coupling constant. The anomalous $\mathrm{U_A}(1)$ transformation induces the following additional contribution,

$$\begin{aligned}\mathcal{L}'_\theta &= \frac{g_s^2}{16\pi^2}(\theta + \arg\ \det \hat{m}^*)\epsilon^{\mu\nu\rho\sigma}F^a_{\mu\nu}F^a_{\rho\sigma} \\ &= \frac{g_s^2}{16\pi^2}(\theta + \pi)\epsilon^{\mu\nu\rho\sigma}F^a_{\mu\nu}F^a_{\rho\sigma},\end{aligned} \tag{A2}$$

with $\hat{m}^* = \mathrm{diag}(m_u^*, m_d^*, m_s^*)$. In evaluating the second line, we assume that all the constituent quark masses are negative. The term breaks *CP* symmetry and generates the neutron electric dipole moment. The coefficient is experimentally constrained as in Ref. [43],

$$\theta + \pi \lesssim 10^{-9}. \tag{A3}$$

This is a fine-tuning problem, which is known as the strong *CP* problem [44].

Then the *CP* symmetry is almost restored after the chiral condensation. The primordial θ may be tested in the phenomena at high T and μ, where the chiral symmetry is partially restored. One of these possibilities may be found in the process for the baryongenesis, but it is beyond the scope of the present study based on the NJL model.

[1] For recent reviews, M. A. Stephanov, Prog. Theor. Phys. Suppl. **153**, 139 (2004); Int. J. Mod. Phys. A **20**, 4387 (2005); Proc. Sci. LAT (2006) 024; O. Philipsen, Prog. Theor. Phys. Suppl. **174**, 206 (2008); Acta Phys. Pol. B Proc. Suppl. **5**, 825 (2012); W. Weise, Prog. Theor. Phys. Suppl. **186**, 390 (2010); Prog. Part. Nucl. Phys. **67**, 299 (2012); K. Fukushima and T. Hatsuda, Rep. Prog. Phys. **74**, 014001 (2011); G. Endrodi, Z. Fodor, S. D. Katz, and K. K. Szabo, J. High Energy Phys. 04 (2011) 001.
[2] Y. Nambu and G. Jona-Lasinio, Phys. Rev. **122**, 345 (1961); **124**, 246 (1961).
[3] K. Fukushima, Phys. Lett. B **591**, 277 (2004).
[4] M. Gell-Mann and M. Levy, Nuovo Cimento **16**, 705 (1960).
[5] J. Gasser and H. Leutwyler, Nucl. Phys. **B250**, 465 (1985).
[6] K. G. Wilson, Phys. Rev. D **10**, 2445 (1974).
[7] U. Vogl and W. Weise, Prog. Part. Nucl. Phys. **27**, 195 (1991).
[8] S. P. Klevansky, Rev. Mod. Phys. **64**, 649 (1992).
[9] T. Hatsuda and T. Kunihiro, Phys. Rep. **247**, 221 (1994).
[10] M. Buballa, Phys. Rep. **407**, 205 (2005).
[11] U. Wolff, Phys. Lett. **157B**, 303 (1985).
[12] T. Hatsuda and T. Kunihiro, Phys. Rev. Lett. **55**, 158 (1985).

[13] F. Karsch, J. B. Kogut, and H. W. Wyld, Nucl. Phys. **B280**, 289 (1987).
[14] K. G. Klimenko, Z. Phys. C **37**, 457 (1988).
[15] M. Asakawa and K. Yazaki, Nucl. Phys. **A504**, 668 (1989).
[16] B. Rosenstein, B. Warr, and S. H. Park, Phys. Rep. **205**, 59 (1991).
[17] S. Hands, A. Kocic, and J. B. Kogut, Nucl. Phys. **B390**, 355 (1993).
[18] P. Zhuang, J. Hufner, and S. P. Klevansky, Nucl. Phys. **A576**, 525 (1994).
[19] T. Inagaki, T. Kouno, and T. Muta, Int. J. Mod. Phys. A **10**, 2241 (1995).
[20] J. Berges and K. Rajagopal, Nucl. Phys. **B538**, 215 (1999).
[21] K. Fukushima, Phys. Rev. D **68**, 045004 (2003).
[22] C. Ratti, M. A. Thaler, and W. Weise, Phys. Rev. D **73**, 014019 (2006).
[23] S. Roessner, C. Ratti, and W. Weise, Phys. Rev. D **75**, 034007 (2007).
[24] K. Fukushima, Phys. Rev. D **77**, 114028 (2008); **78**, 039902(E) (2008).
[25] T. Hell, S. Roessner, M. Cristoforetti, and W. Weise, Phys. Rev. D **79**, 014022 (2009); **81**, 074034 (2010).
[26] S. Krewald and K. Nakayama, Ann. Phys. (N.Y.) **216**, 201 (1992); T. Inagaki, T. Kouno, and T. Muta, Int. J. Mod. Phys. A **10**, 2241 (1995).
[27] S. I. Kruglov, Hadronic J. **26**, 425 (2003).
[28] R. G. Jafarov and V. E. Rochev, Russ. Phys. J. **49**, 712 (2006).
[29] T. Fujihara, D. Kimura, T. Inagaki, and A. Kvinikhidze, Phys. Rev. D **79**, 096008 (2009).
[30] T. Inagaki, D. Kimura, H. Kohyama, and A. Kvinikhidze, Phys. Rev. D **85**, 076002 (2012).
[31] T. Inagaki, D. Kimura, H. Kohyama, and A. Kvinikhidze, Phys. Rev. D **83**, 034005 (2011).
[32] T. Inagaki, D. Kimura, and A. Kvinikhidze, Phys. Rev. D **77**, 116004 (2008).
[33] T. Fujihara, T. Inagaki, D. Kimura, and A. Kvinikhidze, Prog. Theor. Phys. Suppl. **174**, 72 (2008).
[34] M. Kobayashi and T. Maskawa, Prog. Theor. Phys. **44**, 1422 (1970); M. Kobayashi, H. Kondo, and T. Maskawa, Prog. Theor. Phys. **45**, 1955 (1971).
[35] G. 't Hooft, Phys. Rev. D **14**, 3432 (1976); **18**, 2199(E) (1978); Phys. Rep. **142**, 357 (1986).
[36] M. A. Shifman, Prog. Theor. Phys. Suppl. **131**, 1 (1998).
[37] R. F. Dashen, Phys. Rev. D **3**, 1879 (1971).
[38] T. Eguchi, Phys. Rev. D **17**, 611 (1978).
[39] O. Scavenius, A. Mocsy, I. N. Mishustin, and D. H. Rischke, Phys. Rev. C **64**, 045202 (2001).
[40] S. B. Ruester, V. Werth, M. Buballa, I. A. Shovkovy, and D. H. Rischke, Phys. Rev. D **72**, 034004 (2005).
[41] F. R. Brown, F. Butler, H. Chen, N. Christ, Z. Dong, W. Schaffer, L. Unger, and A. Vaccarino, Phys. Rev. Lett. **65**, 2491 (1990).
[42] R. D. Pisarski and F. Wilczek, Phys. Rev. D **29**, 338 (1984).
[43] J. Beringer *et al.* (Particle Data Group), Phys. Rev. D **86**, 010001 (2012).
[44] H.-Y. Cheng, Phys. Rep. **158**, 1 (1988).